The influence of boundary conditions in a reservoir model on the accuracy of the simulation results

Bo Jin[1]

[1]Department of Earth Resources Engineering, Kyushu University, No. 418 West Building 2, Fukuoka, Japan

jin.bo.115@s.kyushu-u.ac.jp

Keywords: *Boundary condition, cell volume, volume factor, upflow.*

ABSTRACT

A geothermal system could include multiple geothermal fields, and it is common to find later that such separate fields are associated. Therefore, when developing a reservoir model, it is a prudent strategy to include the entire geothermal system to leave the potential for further modifications in the future. However, acquiring the necessary data for all the fields or constructing the whole model from the beginning can be difficult.

In this research, the Domes field, a part of the Olkaria geothermal system in Kenya, is extracted from the entire model and used for detailed construction. This paper will introduce how the unsymmetrical block sizes on the borders of the model influence the fluid flow in the reservoir. It also discusses techniques for making modifications along with calibration strategies considering fluid inflow from neighboring fields.

1. INTRODUCTION

Most areas of geothermal activity are given geographic names. Provided they are distinct and separate from neighboring areas of activity, they have been described as geothermal fields. The many fields in the world that have double names (Mak-Ban, Karaha-Bodas, Bacon-Manito) illustrate that exploration has shown that surface activity originally thought to be associated with separate fields is later found to be part of a single, larger field (Grant and Bixley, 2011).

The research subject, Olkaria geothermal system, is located in the Kenya Rift Valley, part of the tectonically active East African Rift Valley. It is divided into seven subsectors: Olkaria East, Olkaria Northeast, Olkaria Southeast, Olkaria Central, Olkaria Northwest, Olkaria Southwest, and Olkaria Domes (Figure 1) (Rop, 2013).

At the current stage of this research, only the Domes field will be considered for detailed simulations. However, when constructing the initial numerical model, the entire Olkaria geothermal system will be included to leave the potential for modifications in the future as each subfield may interact with each other. The boundary of the initial Olkaria model covers a 20 km × 14 km area, which includes the entire Olkaria geothermal system (Figure 3a). It will result in the Domes field model having unsymmetrical cell sizes on the boundaries, which are more extensive in the east and south and finer in the north and west (Figure 3b).

This research aims to evaluate the influence of such uncommon boundary cell sizes on the simulation result and develop the required techniques for calibration using the software Petrasim. Moreover, to assess the impact of inflow from neighboring fields on the model's boundary temperatures to prove the necessity of constructing a big model that includes the entire geothermal system from the beginning.

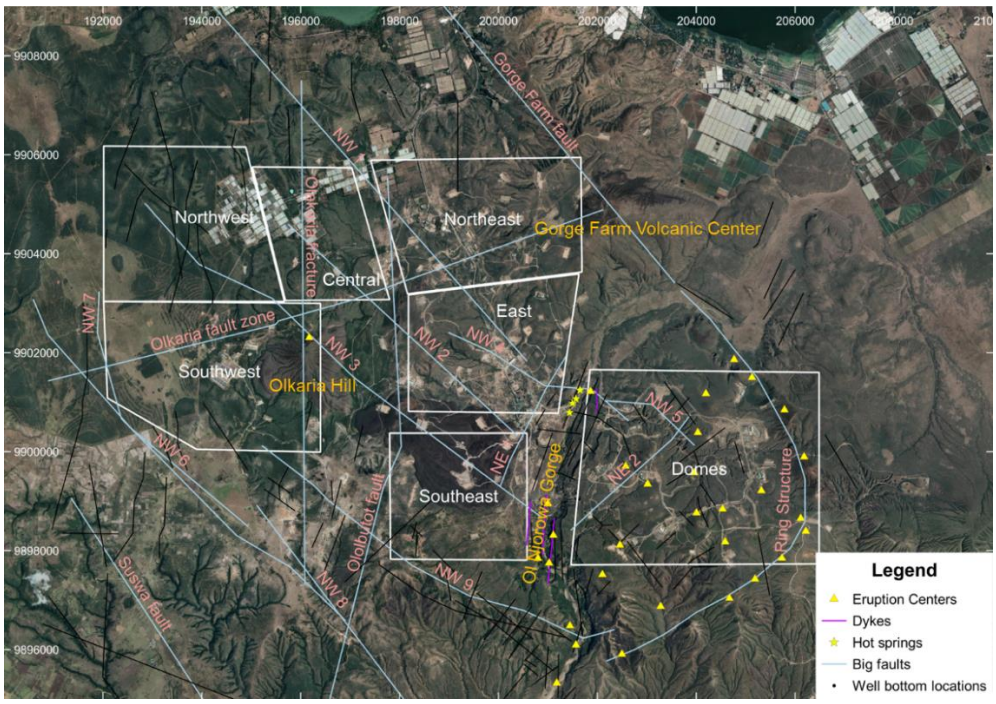

Figure 1. The Olkaria geothermal system's seven subsectors and major fault systems' locations.

Proceedings 45th New Zealand Geothermal Workshop
15-17 November, 2023
Auckland, New Zealand
ISSN 2703-4275

2. CONCEPTUAL MODEL

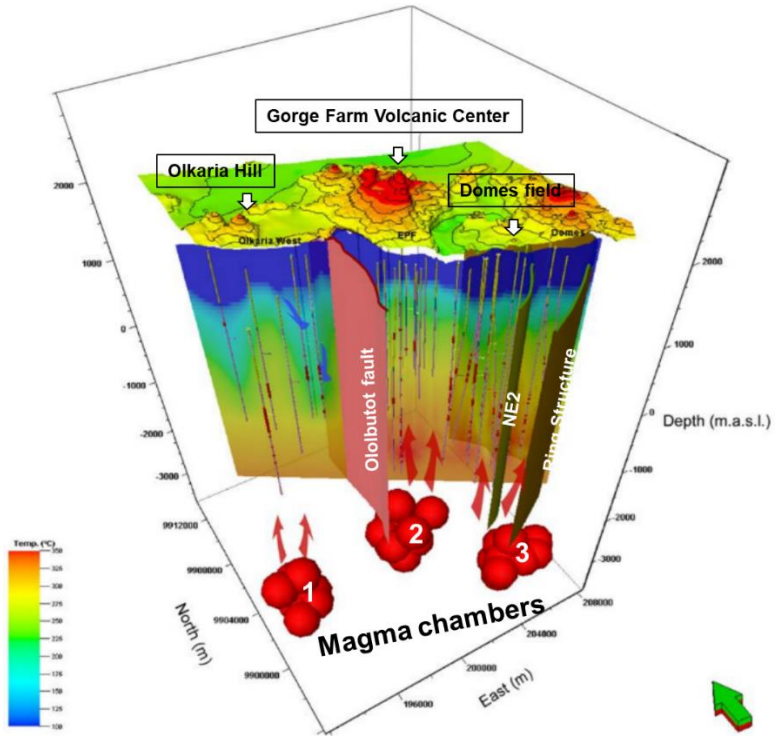

Figure 2. Conceptual model of Olkaria (Modified from Rop, 2013 and Mannvit/ÍSOR/Vatnaskil/Verkís, 2011).

The present conceptual model of the Olkaria geothermal system was developed in 2012 by a consortium of Mannvit/ÍSOR/Vatnaskil/Verkís. According to this model, the heat source is believed to be a deep-seated magma chamber or several chambers with three intrusions 6-8 km from the surface, lying beneath 1) the Olkaria Hill, 2) the Gorge farm volcanic center, and 3) the Olkaria Domes area (Figure 2). Four major upflow zones were identified. The first feeds the Olkaria West field, believed to relate to the heat source beneath Olkaria Hill. Two major up-flow zones were identified as being connected to the Gorge farm heat source, one feeding the Northeast production field and another providing the East field and the northeast corner of the Domes field. The fourth up-flow zone is associated with the ring structure in the Domes field, connected to the heat source identified below that area (Figure 1) (Rop, 2013).

Permeability is believed to be controlled by NW-SE, NE-SW trending faults, and the ring structure. Cold water flows into the system through the N-S trending Ololbutot fault, a flow barrier between the western and eastern parts of the field. Water inflow into the Olkaria Domes area is believed to originate from the northeast part of the Domes field (Figure 1) (Rop, 2013).

3. NUMERICAL MODEL

The numerical model of Olkaria was constructed using the software Petrasim, which is an interactive preprocessor and post-processor for the TOUGH family of codes. It helps users rapidly develop models and view results for these general purpose simulations, which model nonisothermal flows of multicomponent, multiphase fluids in porous and fractured media (RockWare, 2022). In this research, the simulation selected the module of EOS1, which is specified for simulating pure water in its liquid, vapor, and two-phase states (Pruess et al., 1999).

3.1 Layers and Grid System

The model's surface starts from 2000 m a.s.l. and consists of 18 layers with a bottom layer depth of -1500 m a.s.l. Except for the 100 m thickness of the first layer, the rest 17 layers have a uniform thickness of 200 m.

Table 1. Meshing design of the Olkaria model.

Direction	Number of Cells	Cell Size (m)
X	2	1000
	1	500
	70	200
	1	500
	3	1000
Y	2	1000
	50	200
	2	1000

The full scale of the Olkaria model has a dimension of 20 km × 14 km for the W-E and the S-N direction, respectively, with a depth of 3500 m from the surface layer to the bottom of the model. It corresponds to 280 km^2 of area (Figure 3a). The Domes field has a 9.7 km x 8.6 km dimension in the W-E and S-N direction, respectively (Figure 3b). It corresponds to 82.56 km^2 of surface area and 288.96 km^3 of volume. The default meshing order in Petrasim starts from the West (left) to the East (right) and from the North (up) to the South (down), respectively. The specific dimensions and meshing of the model are shown in Table 1. The Olkaria model consists of 79002 cells with a subset of 24570 activated cells for the Domes field. Fine grids were assigned to the center zone for better simulation accuracy.

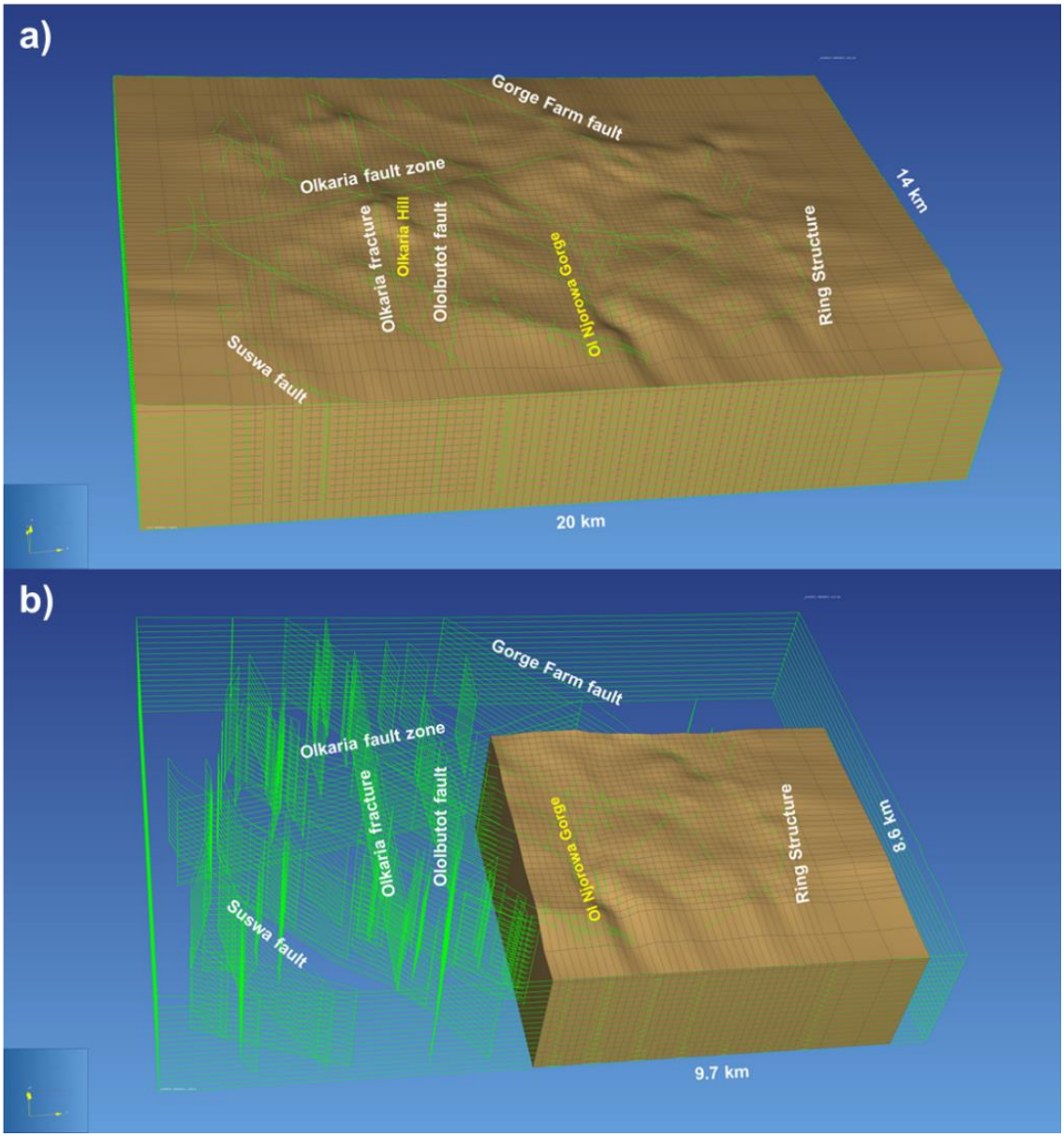

Figure 3. Constructed 3D numerical model. a) Entire Olkaria model. b) Extracted cells for the Domes field model. (Green colors represent major fault systems.)

As time-independent Dirichlet boundary conditions in TOUGH2, for the inactive elements, no mass or energy balance equations are set up, their primary thermodynamic variables are not included in the list of unknowns, and their thermodynamic conditions will remain unchanged. The computational overhead of inactive elements is small because they do not increase the number of equations to be solved in a flow problem (Pruess et al., 1999).

3.2 Rock properties and heat sources

The name of the model used in this research is Model 0, which is a prototype. The primary purpose of this model is to match most wells' pressure gradients with formation pressures by accurately estimating the properties of seven types of rock. These are pyroclastic deposits, rhyolite, tuff, basalt, trachyte, syenitic intrusion, and basaltic intrusion that collectively comprise the Domes field (Table 2.) Further permeability calculations are performed in the horizontal and vertical directions using Weighted-average and Harmonic-average permeability methods based on well-logging information that is assigned to each layer of the model (Figure 4a). Moreover, to match most wells' bottom-hole temperatures with simulated formation temperatures, minimum flow rates of upflow were assigned. The model requires further calibration considering the increase in permeability in the vertical direction caused by fault systems and the decrease in temperature caused by natural cold water recharge, which was accomplished with Model 1 and Model 2 through gradual modification.

The model used two types of heat sources, with both assigned to the bottom layer (Figure 4b). The first heat source is heat flux, with a value of 0.081 J/(s·m²) corresponding to a 40°C/km temperature gradient. The second heat source is upflow, and the total mass flow rate used in Model 0 of this research is 71.6 kg/s with enthalpies of 1800 kJ/kg, corresponding to 363.6°C of saturated water. The properties of additional types of rocks are shown in Table 3.

ISSN 2703-4275

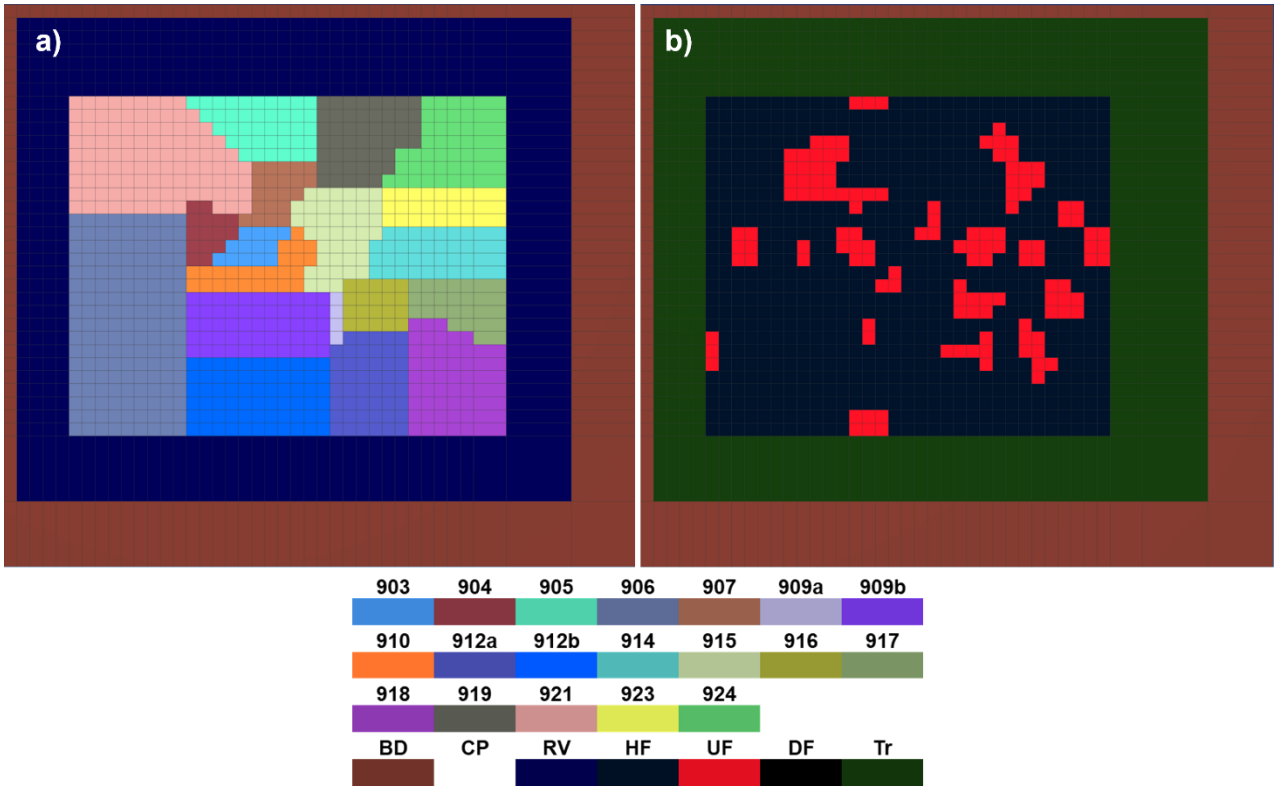

Figure 4. Distribution of rock types for the activated zone. a) Middle layer. b) Bottom layer.

Table 2. Properties of seven types of rocks consisting of Domes field.

Abbreviation	Rock Type	Density	Porosity	Permeability (m^2)			Wet Heat Conductivity	Specific Heat
		(kg/m^3)	(%)	k_x	k_y	k_z	(W/m·K)	(J/kg·K)
Py	Pyroclastic deposit	2700	10	2.5×10^{-15}	2.5×10^{-15}	2.5×10^{-15}	2.0	1000.0
Rh	Rhyolite	2700	10	8.7×10^{-17}	8.7×10^{-17}	8.7×10^{-17}	2.0	1000.0
Tu	Tuff	2700	10	5.0×10^{-17}	5.0×10^{-17}	5.0×10^{-17}	2.0	1000.0
Ba	Basalt	2700	10	6.4×10^{-17}	6.4×10^{-17}	6.4×10^{-17}	2.0	1000.0
Tr	Trachyte	2700	10	6.0×10^{-16}	6.0×10^{-16}	6.0×10^{-16}	2.0	1000.0
I(S)	Intrusion (Syenitic)	2700	10	5.0×10^{-15}	5.0×10^{-15}	5.0×10^{-15}	2.0	1000.0
I(B)	Intrusion (Basaltic)	2700	10	5.0×10^{-15}	5.0×10^{-15}	5.0×10^{-15}	2.0	1000.0

Table 3. Additional types of rocks.

Abbreviation	Full name	Density	Porosity	Permeability (m^2)			Wet Heat Conductivity	Specific Heat
		(kg/m^3)	(%)	k_x	k_y	k_z	(W/m·K)	(J/kg·K)
BD	Boundary	2700	10	1.0×10^{-17}	1.0×10^{-17}	1.0×10^{-17}	0	1000.0
CP	Cap Rock	2700	10	5.0×10^{-17}	5.0×10^{-17}	5.0×10^{-17}	2.0	1000.0
RV	Reservoir	2700	10	5.0×10^{-16}	5.0×10^{-16}	2.5×10^{-16}	2.0	1000.0
HF	Heat flux	2700	10	6.0×10^{-16}	6.0×10^{-16}	6.0×10^{-16}	2.0	1000.0
UF	Upflow	2700	10	6.0×10^{-16}	6.0×10^{-16}	6.0×10^{-16}	3.0	1000.0

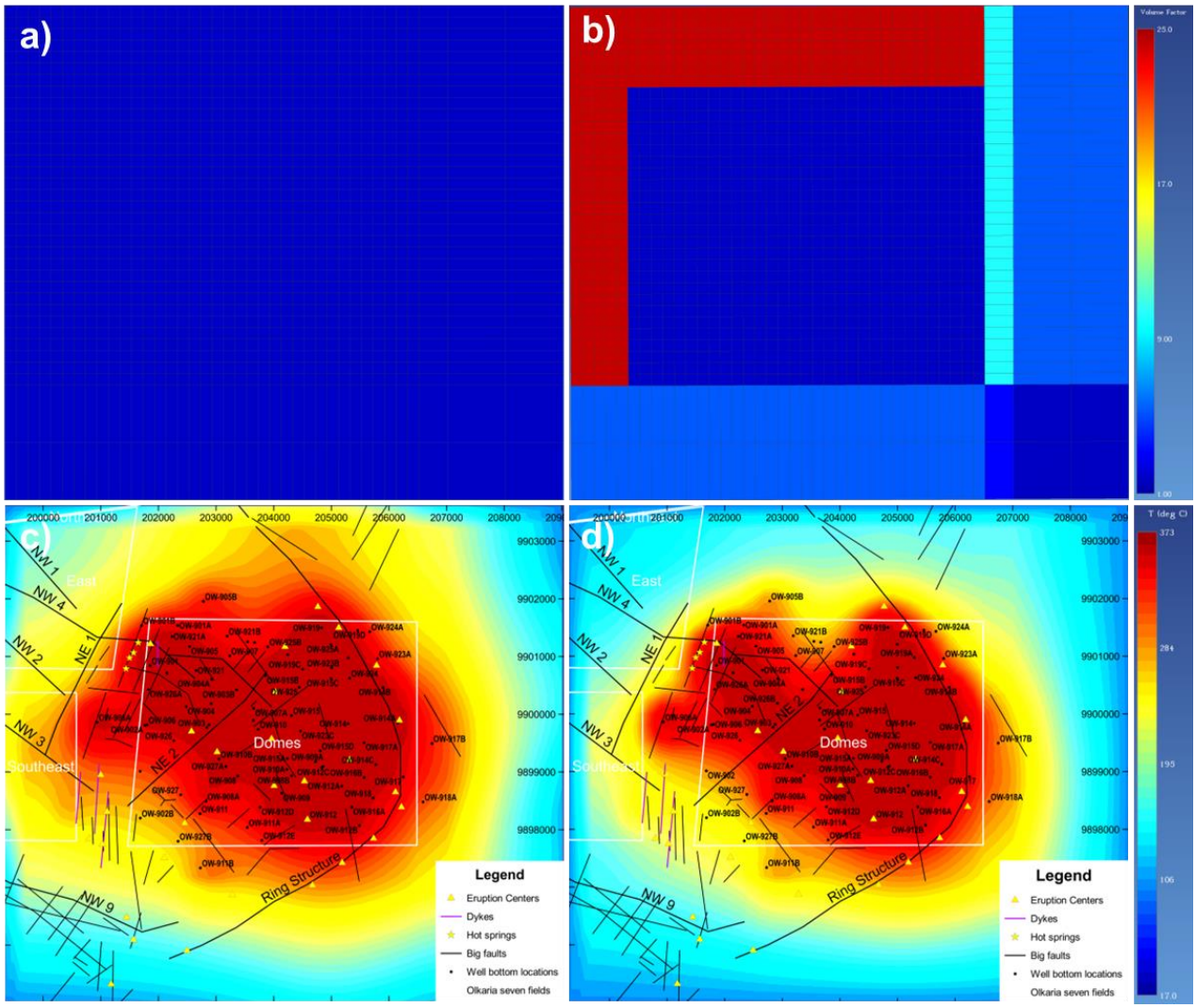

Figure 5. The influence of cell sizes on the boundaries for the simulation results. a) Initial model. b) Calibrated model. c) Temperature contour of the initial model at -1200 m a.s.l. d) Temperature contour of the calibrated model at -1200 m a.s.l.

3.3 Calibration of boundary conditions and results

One of the advantages of establishing a model that includes the entire Olkaria geothermal system is that it can leave potential for the future when enough field data are available to extend the simulation to other fields. The Domes field was the only activated area for the simulation, and the rest of the regions were disabled. However, the boundaries of the entire model and locations of major faults are still visible, which will help calibrate the model based on the conceptual model.

The Domes field, being an extracted part of the full Olkaria model, resulted in North and West cells having smaller volumes than the South and East boundaries (Figure 3b).

Boundary conditions can be of two basic types. Dirichlet conditions prescribe thermodynamic conditions, such as pressure, temperature, etc., on the boundary, while Neumann conditions prescribe fluxes of mass or heat crossing boundary surfaces. Dirichlet conditions can be implemented by assigning very large volumes to grid blocks adjacent to the boundary so that their thermodynamic conditions do not change at all from fluid or heat exchange with finite-size blocks in the flow domain. Time-dependent Neumann conditions can be specified by making sink and source rates time dependent. Time-dependent Dirichlet conditions can also be implemented by placing appropriate sinks or sources in the boundary blocks (Pruess et al., 1999).

For example, consider a laboratory experiment reported by Kruger and Ramey (1974) that involved flashing flow from a sandstone core with a time-dependent gas pressure boundary condition maintained at the outflow end. The equations are shown below:

$$P_b = P_0 + P_1 t + P_2 t \quad \text{(Eq. 1)}$$

$$M_b = P_b\left(\frac{mV}{RT}\right) \quad \text{(Eq. 2)}$$

$$Q_b = \frac{dM_b}{dt} = \left(\frac{mV}{RT}\right)\mathrm{d}\,P_b/dt = \left(\frac{mV}{RT}\right)(P_1 + 2P_2 t) \quad \text{(Eq. 3)}$$

According to the ideal gas law, the pressure behavior of Eq. 1 can be associated with a time-dependent gas inventory of mass M_b in volume V as Eq. 2. Where m is the molar weight of the gas, R the universal gas constant, and T absolute temperature. The required time dependence of M_b can be realized by means of a sink/source rate in Eq3. Therefore, the desired boundary condition can be implemented by means of

ISSN 2703-4275

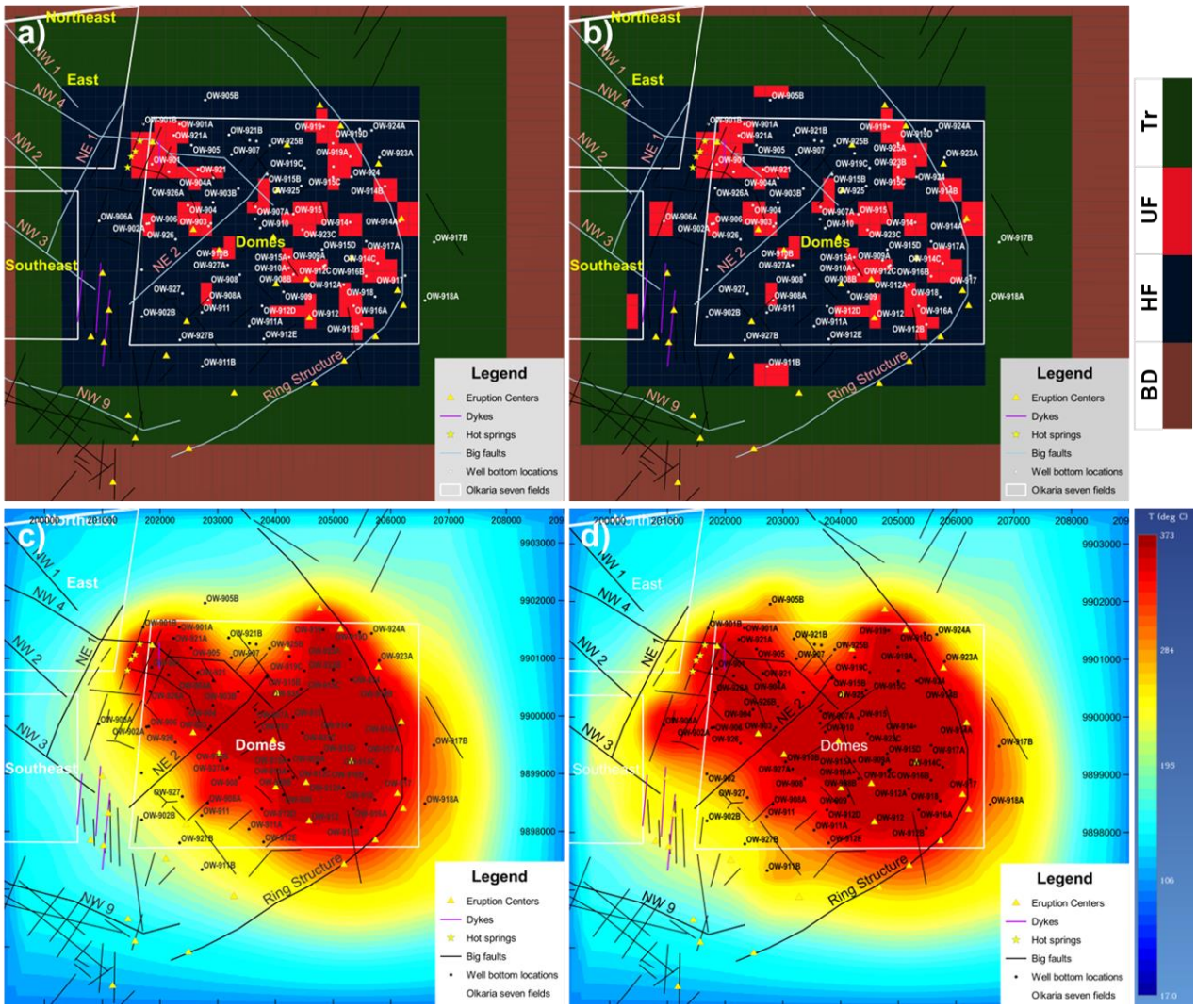

Figure 6. Comparison of temperature contours by assigning additional upflow near boundaries at -1200 m a.s.l. a) Upflow only comes from the divided field. b) Additional upflow comes from outside of the field. c) temperature contour based on upflow distributions of a). d) temperature contour based on upflow distributions of b).

a grid block with volume V that is initialized in single-phase gas conditions, with pressure P_0, and with a time-dependent sin/source term given by Eq. 3. For the pressure conditions in this block to be negligibly affected by heat and mass exchange with the flow domain, volume V should be made very large, just as for time-independent Dirichlet boundary conditions (Pruess et al., 1999). Therefore, increasing the volume of cells on the boundaries is necessary in either case.

To make the volume of the cell with the boundary condition "very large" relative to the other cells in the grid, there is no absolute definition of "very large." However, the concept is that the volume should be so large that flow in and out of the boundary condition cell to model cells will have a negligible effect on temperature or pressure in the boundary condition cell (RockWare, 2022). This research selected the volume of 1.0×10^9 m^3 as boundary conditions, the same as the cell volume in the southeast corner of the original model (Figure 3b). It was accomplished by setting the volume multiplication factor to large numbers, which is a multiplier on the volume that is used to obtain the final volume sent to the TOUGH input file (RockWare, 2022). The specific distributions of the volume factors before and after the calibration are shown in Figures 5a and b.

The comparison of simulation results before and after the calibration is shown in Figures 5c and d, indicating that reservoir fluid will be pushed towards the north and west directions that have small cell sizes without adjustments with volume factors, resulting in increased temperature in the north and west boundaries (Figure 5c).

3.4 Calibration of the model using the upflow near the boundaries

Figures 6a and b show two base layers that provide upflow for the model and are already calibrated with volume factors to increase the volume of boundary cells. White grids represent the division of the field. Compared with Figure 6a, Figure 6b has additional upflow outside the area. The simulation result shows that, with additional upflow from outside the site, the well bottom temperature of well OW-906A near the west boundary better matches the formation temperature (Figure 7). This indicates that the origin of upflow is not limited to the assigned field itself. Therefore, a prudent strategy to construct a model is to cover more areas from the beginning, which could include the entire geothermal system, leaving enough potential for modifications. The comparison of temperature contours is shown in Figures 6c and d.

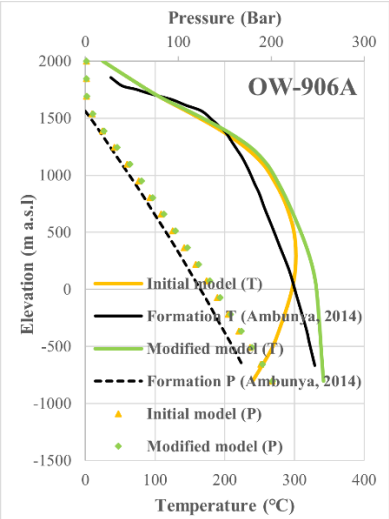

Figure 7. Comparison of temperature distribution for a well near the west boundary before and after modifications.

4. CONCLUSION

The simulation results show that as an essential type of heat source, some upflow could originate from neighboring fields, which further indicates that geothermal fields are often related. Therefore, it is prudent to include the entire geothermal system from the beginning when developing a numerical model. The required field for the modeling could be achieved by inactivating the rest of the fields of the whole model, and the boundary conditions could be established by applying volume factors for cells having small volumes on the boundaries.

ACKNOWLEDGEMENTS

This work was supported by JST SPRING, Grant Number JPMJSP2136.

REFERENCES

Ambunya, M.N., 2014. *Natural-state model update of Olkaria Domes geothermal field.* United Nations University.

Grant, M. A., Bixley, P. F., 2011. *Geothermal Reservoir Engineering, Second Edition.* Academic Press, USA.

Kruger, P. and H.J. Ramey, Jr: *Stimulation and Reservoir Engineering of Geothermal Resources, Stanford Geothermal Program Report SGR-TR-1*, Stanford University, Stanford, CA, 1974.

Mannvit/ÍSOR/Vatnaskil/Verkís Consortium, 2011. *Revision of the conceptual model of the Greater Olkaria Geothermal System-Phase I.* Mannvit/ÍSOR/Vatnaskil/Verkís, Reykjavík, 100pp.

Pruess, K., Oldenburg, C., Moridis, G., 1999. *TOUGH2 USER'S GUIDE, VERSION 2.*

RockWare, 2022. *PetraSim User Manual, USA.* https://www.rockware.com/downloads/documentation /petrasim/ PetraSimManual.pdf.

Rop, E., 2013. *Interpretation of recent temperature and pressure data and updated conceptual model of the Greater Olkaria geothermal system, Kenya.* United Nations University.